8

Response of Continuous Pipelines to Faulting

Chapters 6 and 7 present the response of continuous pipelines subject to longitudinal and transverse PGD, respectively As mentioned previously, arbitrary PGD can be decomposed into two components, one, parallel to pipe axis (i.e , longitudinal PGD) and the other, perpendicular to pipe axis (i e., transverse PGD) This chapter presents the response of continuous pipelines subject to fault offsets, which in the general case involves both longitudinal and transverse response

Two cases are discussed herein In Case I, pipes are distressed due to bending (caused by transverse component) and axial tensile force (caused by longitudinal component) A normal fault and strike-slip fault with the intersection angle between the fault trace and the pipe axis, β (shown in Figure 8.1), less than 90° are examples of this case. The pipe failure mechanism would be tensile rupture since the fault offset results primarily in tensile strain in the pipe in this case.

In Case II, pipes are distressed due to bending and axial compressive force. A reverse fault and strike-slip fault with the intersection angle, β, between the fault trace and the pipe axis more than 90° are examples of this case. The pipe failure mechanism would be buckling since this type of fault results primarily in compressive strain in the pipe in this case

Surface faulting has accounted for many pipe breaks during past earthquakes. For example, much of the surface faulting during the 1971 San Fernando earthquake occurred in urban and suburban communities. Although only a half of one percent of the area was influenced by the surface faulting, the fault movements resulted in over 1,400 breaks in water, natural gas and sewer pipelines (McCaffrey and T O'Rourke, 1983). Among the three fault zones (the Mission Wells segment, the Sylmar segment and the Harding school segment), the 3 km long (1.9 mile) Sylmar segment had the largest ground displacement which was composed

of 1.9 m (6.2 ft) of left-lateral slip, 1.4 m (4.6 ft) of vertical offset and 0.6 m (2.0 ft) of thrust. Most of the left-lateral slip and thrust were concentrated along the southern 25 to 80 m wide (82 to 262 ft) section of the fault zone, where the failure mode of local buckling to the pipe wall was dominant. On the other hand, vertical offsets and extension fractures are predominant in the northern section, where most of the breaks were due to tensile failure.

There are three potential failure modes for a continuous pipeline fault crossing. They are: tensile rupture, local buckling (wrinkling) in compression, and beam buckling in compression. The beam buckling mode is discussed in detail in Section 4.1.3. As noted pipelines are typically buried about 1.0 m (3.0 ft) below the ground surface. Since this burial depth is larger than the critical burial depth shown in Figure 4.5, the pipe wrinkles rather than buckles like a beam when subject to compressive PGD. Hence, this chapter focuses on tensile rupture of a pipe due to bending and tension, and wrinkling of the pipe wall due to bending and compression.

8.1 STRIKE SLIP FAULT

A number of investigations have been performed regarding tensile and bending behavior due to large abrupt fault movements. These include: the Newmark-Hall (1975) approach, the Kennedy et al. approach, and the Wang-Yeh (1985) approach. Herein these analytical approaches are reviewed and the results are compared to those from an FE model, in which both pipe material nonlinearity as well as the nonlinear interaction at the pipe-soil interface are considered.

8.1.1 ANALYTICAL MODELS

Newmark and Hall (1975) apparently were the first to analyze the fault crossing problem. They considered the model shown in Figure 8.1 with a total fault movement δ_n in which a pipeline intersects a right lateral strike-slip fault at an angle β. For a pipe-fault intersection angle $\beta \leq 90°$, the strike-slip fault results primarily in

tensile strain in the pipe. They assume that the pipe is firmly attached to the soil (i.e., no relative displacement between pipe and soil) at two anchor points located at L_a from the fault trace. Anchors correspond to elbows, tie-ins, and other features, which develop substantial resistance to axial movement.

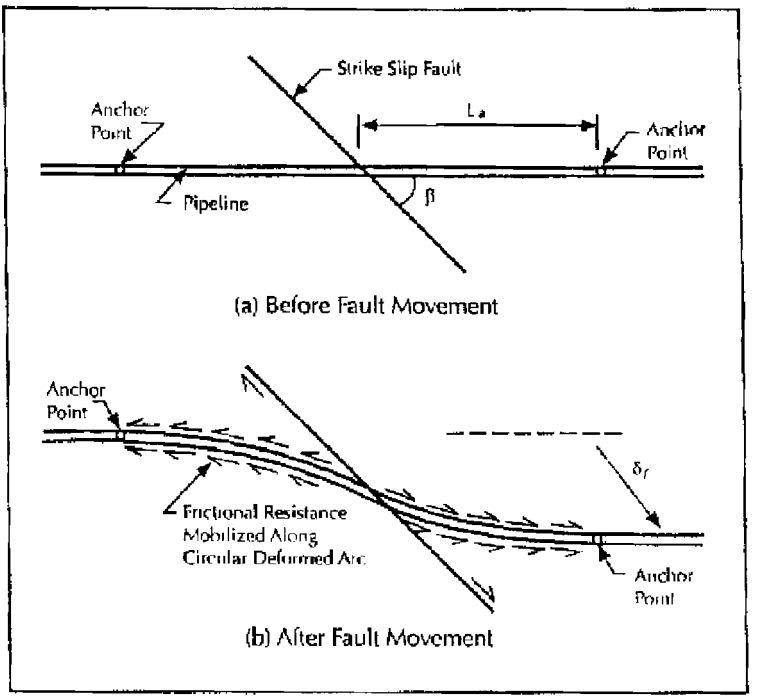

After Newmark and Hall, 1975

Figure 8.1 Plan View of the Newmark-Hall Model for Pipeline Crossing a Right Lateral Strike-Slip Fault

The authors neglect the bending stiffness of the pipe as well as lateral interactions at the pipe-soil interface. That is, they envision a trench with sloping side walls for which only longitudinal interaction at the pipe-soil interface is considered. The total elongation of the pipe is composed of two components. The first is due to the axial component of fault movement ($\delta_f \cos\beta$). The second is due to arc-length effects caused by lateral component of fault movement ($\delta_f \sin\beta$).

Because of symmetry, only one side of the fault trace is considered. The average pipe strain, $\bar{\varepsilon}$, is:

$$\bar{\varepsilon} = \frac{\delta_t}{2L_a}\cos\beta + \frac{1}{2}\left(\frac{\delta_t}{2l_s}\sin\beta\right)^2 \qquad (8.1)$$

where L_a is the effective unanchored length, that is, the distance between the fault trace and the anchor point.

When no bends, tie-ins or other constraints are located near the fault, the friction forces at the pipe-soil interface provide all the axial resistance. In this case, L_a can be estimated by:

$$L_a = L_e + L_p \qquad (8.2)$$

where L_e is the pipe length over which elastic strain develops, while L_p is the length over which plastic strain develops.

L_e, L_p are given by:

$$L_e = (E_i \varepsilon_y \pi D t)/t_u \qquad (8.3)$$

$$L_p = [E_p(\varepsilon - \varepsilon_y)\pi D t]/t_u \qquad (8.4)$$

where ε_y is the yield strain of material, E_i and E_p are the modulus before yield and after yield, ε is the plastic tensile strain in the pipe and t_u is the axial friction force per unit length at the pipe-soil interface. Failure in the Newmark and Hall approach is assumed to occur when the average strain $\bar{\varepsilon}$ is greater than 4%.

For a 0.61 m diameter (24 in) pipe made of X-60 steel, the relation between the tolerable fault movement and the intersection angle using the Newmark and Hall approach is shown in Figure 8.12 along with similar information from other approaches which will be discussed later. The Newmark and Hall model provides valuable insight into the mechanics of this problem, and allows one to evaluate the most influential parameters. However, as will be shown later, this approach over-estimates the tolerable fault movement for pipelines since it uses the average strain as a failure criterion and neglects the lateral interaction at the pipe-soil interface.

Kennedy et al. (1977) extended the ideas of Newmark and Hall, and incorporated some improvements in the method for evaluating the maximum axial strain. They considered the effects of lateral interaction in their analysis. Also, the influence of large axial strains on the pipe's bending stiffness is considered. That is, the pipe bending stiffness becomes very small (roughly 0.5% of the initial stiffness) when axial strain is well beyond the yield strain. As a result, the bending strain in the pipe is relatively small in this approach.

Figure 8.2 presents the Kennedy et al. model, in which the bending strain occurs in the curved region where a constant curvature, $1/R_c$, is assumed.

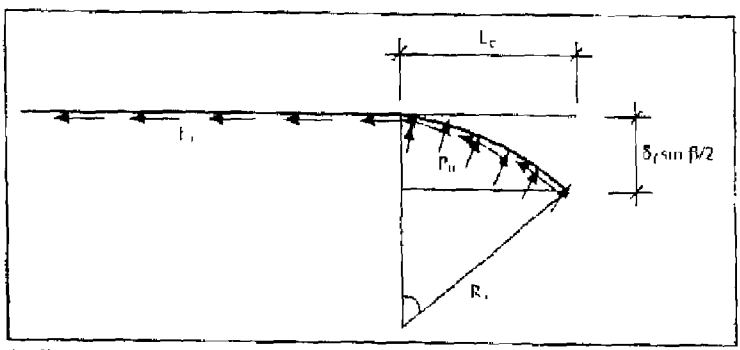

After Kennedy et al., 1977

Figure 8.2 Kennedy et al. Model

The bending strain, ε_b, is expressed as:

$$\varepsilon_b = \frac{D}{2R_c} \tag{8.5}$$

R_c is the radius of curvature of the curved portion, which can be evaluated by using an analogue to internal pressure in a cylinder

$$R_c = \frac{\sigma \pi D t}{P_u} \tag{8.6}$$

where σ is the axial stress at fault crossing, p_u is the lateral soil-pipe interaction force per unit length (see Equation 5.5 for sand or Equation 5.7 for clay).

The total strain in the pipe is given by:

$$\varepsilon = \varepsilon_a + \frac{D}{2R_c} \tag{8.7}$$

where ε_a is the maximum axial strain due to the elongation of the pipe induced by the fault offset.

The total elongation of the pipe, ΔL, can be estimated by:

$$\Delta l = \delta_f \cos\beta + \frac{(\delta_f \sin\beta)^2}{3L_c} \tag{8.8}$$

where the first term is the elongation due to the axial component of the fault movement, while the second term is the elongation due to arc-length effects induced by the lateral component of the fault movement, and L_c is the horizontal projection length of the laterally deformed pipe shown in Figure 8.2, which can be approximated by:

$$L_c = \sqrt{R_c \delta_f \sin\beta} \tag{8.9}$$

Based on the Ramberg Osgood relation in Equation 4.1, the total elongation can be expressed in terms of an integral of axial strain. That is,

$$\Delta L = \frac{2}{F}\int_0^{L_c} \sigma\left[1 + \frac{n}{1+r}\left(\frac{\sigma}{\sigma_y}\right)^r\right] dx \tag{8.10}$$

Integrating Equation 8.10, one can obtain the relation between the axial movement and effective length L_c. Combining Equation 6.3, Equation 6.4 and Equation 8.8, one can obtain the relation between fault offset and pipe strain for any intersection angle β, which is shown later in Figure 8.12.

Figure 8.3 shows the tolerable fault movement for a 42 in (1.07 m) diameter pipe as a function of unanchored length. The critical tensile strain is 4.5% for Hc = 0.9 m and 3.5% for Hc = 3.0 m due to the substantial increase in bending strains and hoop ovaling for the deeper burial depth. The pipe wall thickness is 0.014 m (0.55 in); it's made of X-60 steel and surrounded by loose to moderately dense sand with $\gamma = 1.76 \times 10^4$ N/m^3 (110 pcf) and $\phi = 34°$. The burial depth is 0.91 m (3 ft) from the ground surface to the top of the pipe

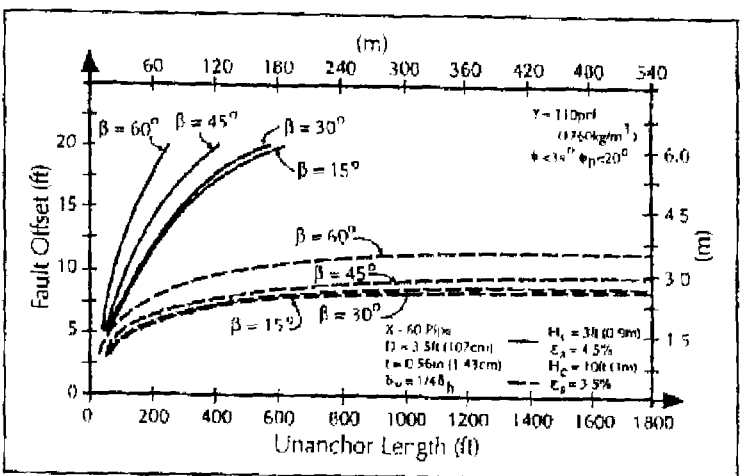

After Kennedy et al, 1977

■ Figure 8.3 Tolerable Fault Movement vs. Unanchored Length

As shown in Figure 8.3, the tolerable fault offset for the pipe is an increasing function of unanchored length and pipe-fault intersection angle, but a decreasing function of burial depth. For the pipe-fault intersection angle of β = 60°, Figure 8.4 shows the maximum axial strain as a function of unanchored length.

As shown in Figure 8.4, the pipe axial strain is a decreasing function of the wall thickness and unanchored length. For a given wall thickness, the axial strain is an increasing function of the pipe diameter, which is due to the corresponding increase in the interaction forces at the pipe-soil interface. In contrast to the Newmark and Hall approach, the authors consider both the axial and lateral interactions at the pipe-soil interface.

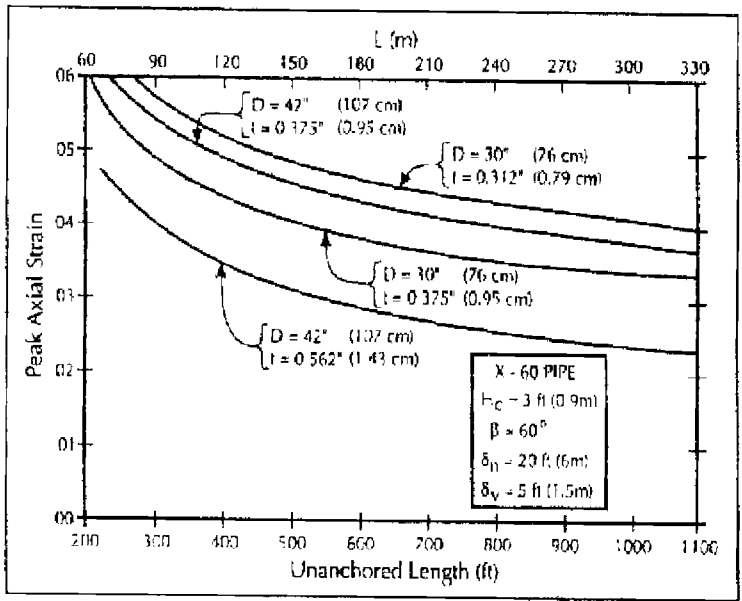

After Kennedy et al 1977

■ **Figure 8.4 Maximum Axial Strain vs Unanchored Length**

Subsequent to the above studies, Wang and Yeh (1985) introduced some additional modifications. The plan view of half of the pipe for Wang-Yeh's model is shown in Figure 8.5

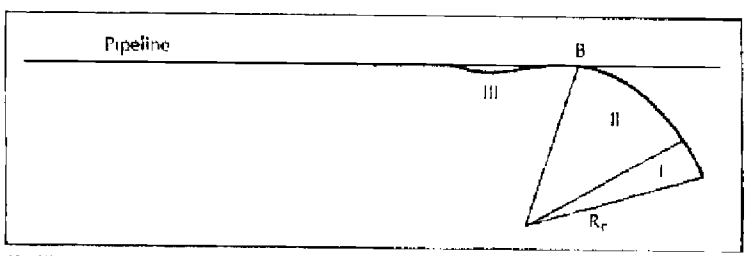

After Wang and Yeh 1985

■ **Figure 8.5 Plan View of Pipeline Crossing Strike-slip Fault**

Assuming a constant radius of curvature for the curved portions (i.e., Regions I and II), Wang and Yeh analyze pipe strain based on the equilibrium of forces and deformation compatibility. They also assume that the strains in Regions II and III are elastic,

while the strains in Region I are inelastic. For the nominally straight portion of the pipe (Region III), a beam on an elastic foundation theory is used.

For a 1.06 m diameter pipe with 0.014 m in wall thickness, made of X-70 steel and surrounded by loose to moderately dense sand ($\gamma = 1.76\times10^4$ N/m^3 (110 pcf), and $\phi = 34°$) with burial depth of 0.91m (3ft) from the ground surface to the top of the pipe, their approach results in the tolerable fault offset of 3.5 m (11.5 ft) for $\beta = 70°$ and 4.6 m (15 ft) for $\beta = 79°$. Note that Wang and Yeh assume that the friction angle at the pipe-soil interface is 20°

Wang and Yeh apparently neglect the influence of pipe axial stress on pipe bending stiffness, and use the initial modulus to evaluate the bending strain in Regions II and III. As a result, they overestimate pipe bending strain in Region II and conclude that the pipe fails at the Point B as shown in Figure 8.5. This seems counterintuitive since one expects tensile ruptures at or very near the fault crossing location.

8.1.2 Finite Element Models

Assuming a constant radius of curvature for the curved portion of the pipe, Ariman and Lee (1991) evaluated pipe strain using the finite element method. The pipe is modeled as a thin cylindrical shell which is essentially semi-infinite. For a 42 in diameter pipe made of X-60 steel, they present the bending strain as a function of soil angle of shearing resistance, burial depth, and pipe diameter in Figure 8.6 (a), (b) and (c) respectively. The amount of fault offset is 6.1 m and the intersection angle is 70° in their calculation.

As shown in Figure 8.6, the Ariman and Lee model suggests that the bending strain in the pipe is an increasing function of the soil friction angle, burial depth and pipe diameter.

For a pipe fault crossing at a right angle (i.e., $\beta = 90°$), Meyersohn (1991) evaluates the pipe strain by a finite element program UNIPIP (Tawfik and T. O'Rourke, 1986). Meyersohn's numerical simulations are performed on two pipelines with burial depth of 0.91 m (3 ft) from top of pipe to the ground surface. Pipe 1, with an outside diameter of 1.06 m (42 in) and a wall thickness of 14 mm (0.55 in), and Pipe 2 with a diameter of 0.3 m (12 in) and a wall thickness of 9.5 mm (3/8 in), are unpressurized and made of X-60 steel. Figure 8.7 shows the maximum compressive

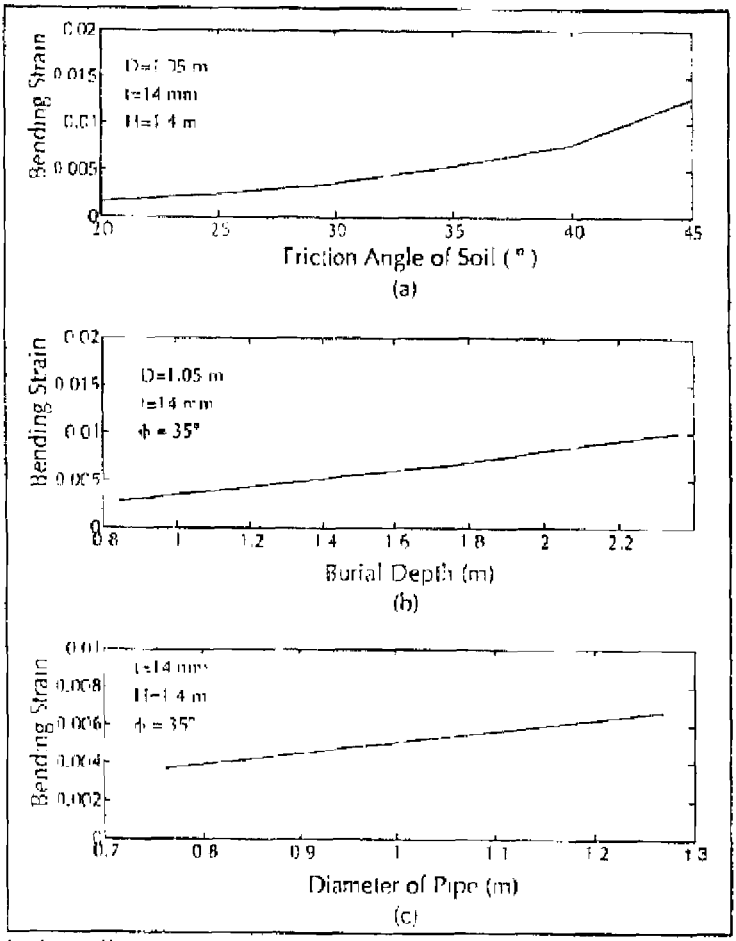

After Ayman and Lee (1991)

■ **Figure 8.6 Pipe Bending Strain as a Function of Soil Friction Angle, Burial Depth and Pipe Diameter**

strain versus the fault displacement, in which the compressive strain generally increases with an increase in the fault displacement. After the displacement reaches a certain value (for example 2.3 m for Pipe 2), the maximum compressive strain decreases with increase of the displacement since the axial tensile strain becomes larger than yield strain due to the arc-length effects induced by the fault movement, according to Meyersohn (1991).

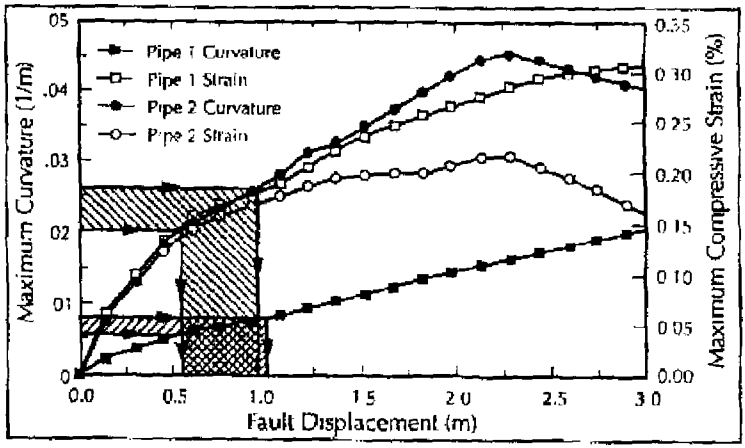

After Meyersohn, 1991

■ *Figure 8.7 Maximum Pipe Compressive Strains as a Function of Fault Offset*

The maximum compressive strain in Figure 8.7 is less than the critical wrinkling strain for the pipes given by Equation 4.3

In order to evaluate the various approaches, the model shown in Figure 8.8 is used herein to estimate the pipe strain using the ABAQUS finite element program

As shown in Figure 8.8, the pipeline model is fixed at the point A, which is 500 m (1640 ft) away from the pipe-fault intersection (Point O). This unanchored length is sufficiently long such that both axial strain and bending strain are zero at point A (i.e., the fixed end). Similarly, there is no relative movement between the pipe and the surrounding soil at Point D (i.e., the unrestrained end). All the bases of soil springs to the left of fault trace are fixed. To the right of the fault trace, all the bases of lateral soil springs

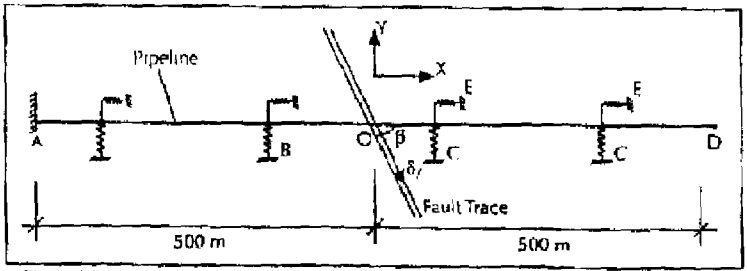

■ *Figure 8.8 Finite Element Model For Pipeline Crossing Strike-slip Fault*

(e.g., Point C) move a distance of $\delta_f \sin\beta$ in the Y direction, while all the bases of axial soil springs (e.g., Point E) move a distance of $\delta_f \cos\beta$ in the X direction.

Considering the non-linear interaction at the pipe-soil interface (Equation 5.1 and Equation 5.5) and the Ramberg Osgood stress-strain relationship (Equation 4.1), the response of an X-60 grade pipe (0.61 m in diameter, 0.0095 m in wall thickness) subject to a strike-slip fault is analyzed.

For a pipe-fault intersection angle of 90°, the distribution of maximum pipe strain is shown in Figure 8.9. The maximum axial strain as well as the peak tensile strain occurs at the intersection where the bending strain is zero (i.e., the point of counterflexure). The bending strain near the intersection (within about 30 m) is relatively constant (i.e., relatively constant curvature as assumed in the Kennedy et al. approach). The peak tensile strain due to the combined effects of axial and bending strains occurs at the intersection.

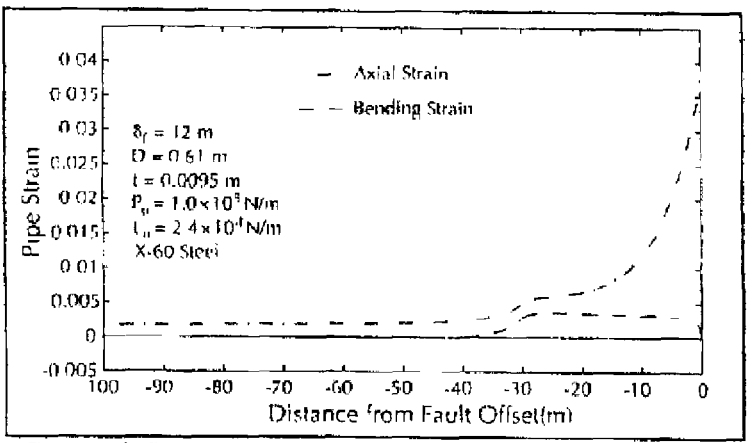

■ Figure 8.9 Distribution of Pipe Strains (for 90° intersection angle)

The peak pipe strain for the same intersection angle (90°) is shown in Figure 8.10 as a function of fault offset.

As shown in Figure 8.10, the peak compression strain occurs for a fault offset of approximately 2 m (6.6 ft) and decreases thereafter. This decrease of compression strain is due to the decrease of bending strain/stiffness caused by the large axial strain. For example, as shown in Figure 8.9 for a fault offset of 12 m (39 ft), the bending strain in the pipe near the fault is a constant value of about 3.6×10^{-3}. Since the axial strain is larger, the net compressive strain is zero.

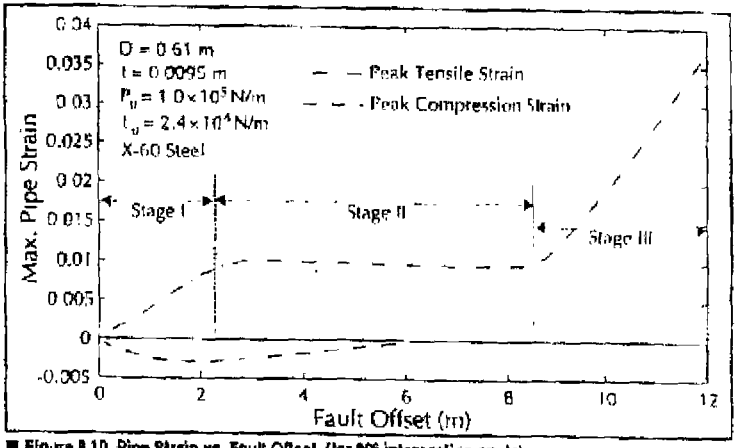

■ Figure 8.10 Pipe Strain vs. Fault Offset (for 90° intersection angle)

Three stages can be identified for the response of a buried pipeline subject to an abrupt lateral fault offset as shown in Figure 8.10. In Stage I (small offsets), both axial and bending strains are important, and both increase with fault offsets. Bending strains are large enough such that there is a non-zero net compressive strain. In Stage II (intermediate offsets), the axial strain is beyond yield, and bending stiffness (and hence bending strain) are decreasing and the net compressive strains approach zero. In Stage III (large offsets), the bending strain remains constant while axial strain increases with increasing fault offsets.

For pipelines made of X-60 and Grade-B steel, the tolerable fault offset is presented in Figure 8.11 as a function of the pipe-fault intersection angle. As shown in Figure 8.11, for an intersection angle less than about 90° (92° for X-60 steel, 90.6° for Grade-B steel), the tolerable fault offset is governed by tensile failure, and increases with the pipe-fault intersection angle. For an intersection angle larger than that angle (Case II), the tolerable fault offset is governed by wrinkling of pipe wall, and the compressive strain reaches the failure criterion at a low value of fault offset. For example, the fault offset of 0.2 m (7.9 in) may cause local buckling to a pipe with 0.61m (24 in) diameter, 0.0095 m (3/8 in) wall thickness and made of Grade-B steel. Note that the solid lines are based on a tensile critical strain of 4%, while the dotted lines are based on a local buckling strain of 0.54% (an average value from Equation 4.3).

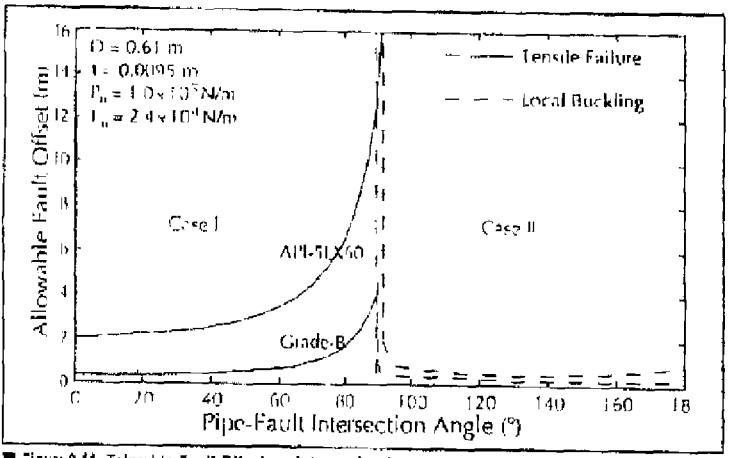

■ Figure 8.11 Tolerable Fault Offset vs. Intersection Angle

8.1.3 COMPARISON AMONG APPROACHES

Figure 8.12 presents the tolerable fault offset from four approaches as a function of the intersection angle between the pipe axis and fault trace.

As shown in Figure 8.12, the results obtained from the ABAQUS numerical approach match that from Kennedy et al.'s analytical approach very well for intersection angles less than 60°. For intersection angles larger than 60°, the tolerable fault offset from the ABAQUS model is somewhat less than that from Kennedy et al.'s approach.

Newmark and Hall's approach overestimates the tolerable fault offset by roughly a factor of 2. This is believed to be due to the use of the average strain for the failure criterion. Note that the maximum strain in the pipe is at least twice the average strain used in their approach. Moreover, they neglect the bending strain in the pipe and the influence of bending strain on the axial stiffness of the pipe. Note that the Newmark and Hall's curve is based on Equation 8.1 with an unanchored length of 50 m (164 ft).

As mentioned previously, for the pipe made of X-70 steel Wang and Yeh's approach leads to tolerable fault offset of 3.5 m (11.5 ft) and 4.6 m (15 ft) for $\beta = 70°$ and $\beta = 79°$, respectively. For the same case, the tolerable fault offset is 15 m (49 ft) for $\beta = 70°$ and

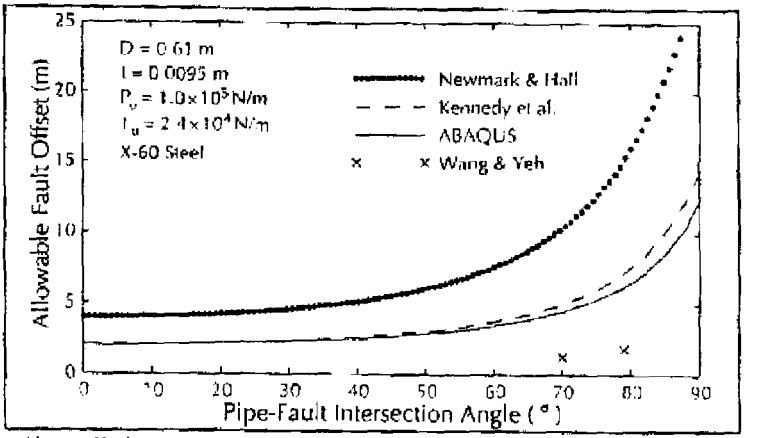

■ Figure 8.12 Comparison of Results from Four Approaches

21 m (69 ft) for β = 79° by Kennedy et al.'s approach which, as noted above, appears to match the finite element results. Hence, Wang and Yeh's approach apparently underestimates the tolerable fault offset for the pipeline by a factor of 4. This is believed to be due to their assumption that the pipe strain in Region II (Figure 8.5) is elastic and a reduced bending stiffness at high axial strain is neglected. In fact, the finite element results suggest that the axial strain in that region does exceed the yield strain and the bending stiffness is, in fact, greatly reduced. Hence, Wang and Yeh's approach overestimates the bending strain in the pipe, and underestimates the tolerable fault offset for the pipe.

Results from the Ariman and Lee model as well as those from Meyersohn are presented in terms of bending strain. Since they also used different diameters and wall thicknesses, no comparison is presented herein.

8.1.4 Comparison With Case Histories

The 1979 Imperial Valley earthquake provides case histories which can be used to benchmark the finite element approach. During this earthquake, three natural gas pipelines were affected by the localized abrupt offsets at the Imperial fault as shown in Figure 8.13. The maximum co-seismic right lateral slip along the

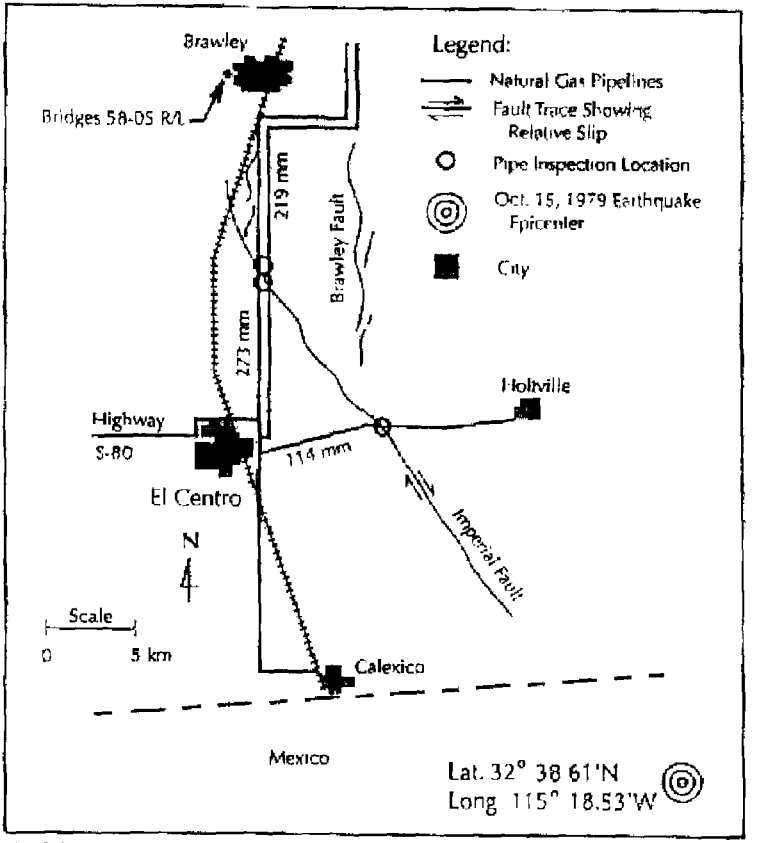

After Roth et al., 1990

■ Figure 8.13 Three Gas Pipelines Intersected by the Imperial Fault

fault was 550 to 600 mm (1.8 to 2.0 ft) at Heber Dunes. Up to 290 mm (1.0 ft) of afterslip was measured at McCale Road 160 days after the earthquake, according to Roth et al. (1990).

The material properties of those pipelines, the amount of fault offset as well as the pipe-fault intersection angles are listed in Table 8.1. The No. 56 coating consists of layers of red oxide primer, filled asphalt, two spiral wraps of cellulose acetate, filled asphalt and paper wrapper. The somastic coating is composed of asphalt, aggregate and fiber mixture. In this case study, Equations 5.1 and 5.5 are used for estimating maximum axial and lateral interacting

force at the pipe-soil interface. We assume the angle of shear resistance of the sand $\phi = 35°$ and $k = 0.7$ for No. 56 coating and $k = 0.9$ for somastic coating.

Two cases are considered herein. In Case I, the fault is assumed to be a single abrupt fault (i.e., the width of offset zone is zero). In Case II, the 9.6 m (32 ft) of actual fault width is used, and linear distribution of ground movement across the width is assumed. The maximum pipe strains from the finite element model as well as the critical strain are listed in Table 8.1. The critical strain for Holtville-El Centro Line (angle 55°) is taken as a tensile rupture strain of 4%, while the critical strains for Lines 6000 and 6001 are taken as the wrinkling strain from Equation 4.3. The predicted behavior matches the observed behavior in that the maximum strain for Case II (actual width used) are less than the critical values, and the pipes did not, in fact, fail. Note that the tensile strains for the Holtville-El Centro Line for both cases are relatively close. However, for the other two pipelines, the compressive strain for the zero-width fault is much larger that for the 9.6 m-wide fault. This suggests that the width of the fault can be a key parameter, particular for compressional movements. That is, the finite element results suggest that the two pipelines in compression would have wrinkled if the width of the fault were small (e.g. less than about 3.0 m (10 ft)).

Table 8.1 Pipe and Fault Properties and Strain Analyses

Characteristic	Holtville-El Centro Line	Line 6000	Line 6001
Diameter	114 mm	219 mm	273 mm
Wall Thickness	5 mm	7 mm	5 mm
Material	A-25 Steel	GR-B Steel	X-42 Stee
Yield Stress	170 MPa	240 MPa	290 MPa
Operating Pressure	2.8 MPa	2.8 MPa	2.8 MPa
Depth of Cover	0.9 m	0.9 m	0.9 m
Weld Type	Acetylene	Electric Arc	Electric Arc
Coating	No. 56	Somastic	No. 56
Fault Offset	0.6 m	0.4 m	0.4 m
Intersection Angle	55°	120°	120°
Max. Tensile Strain (Case I)	0.015	-	-
Max. Tensile Strain (Case II)	0.0126	-	-
Max. Compressive Strain (Case I)	-	> 0.06	0.0335
Max. Compressive Strain (Case II)	-	0.00735	0.00326
Critical Strain	0.04	0.0112	0.0064

Case I, Abrupt offset
Case II, 9.6 m fault width

5.2

Normal and Reverse Fault

Relatively little analytical work has been done for a pipe across a normal or reverse fault. For a pipe subject to a normal fault, the pipe-soil system is no longer symmetric, and the transverse interaction force at the pipe-soil interface for downward movement of the pipeline is much larger than that for upward movement, based on Equation 5.9 to Equation 5.16. Kennedy et al.'s approach can still be used to estimate the pipe strain. In this case, an average lateral interaction force for upward and downward movements can be used to estimate the bending strain from Equations 8.5 and 8.6, and the axial strain is the same as before.

However, for a pipe subject to a reverse fault, it appears that no analytical approach is currently available. The ASCE TCLEE Committee on Gas and Liquid Fuel Lifeline (1984) suggests using the finite element method.

The behavior in such cases is difficult to generalize, in part because there are two angles of intersection (the angle in plan between the fault and the pipeline, as well as the dip angle of the fault) as well as the aforementioned asymmetric nature of the soil resistance in the vertical plane.